



Imaging of the Quiet Sun in the Frequency Range of 20-80MHz

Peijin Zhang*^(1,2,3), Pietro Zucca⁽²⁾, Kamen Kozarev⁽¹⁾, Eoin Carley⁽³⁾, Chuanbing Wang⁽⁴⁾,
and LOFAR SSW-KSP Team⁽²⁾

(1) IANAO-BAS, Sofia 1784, Bulgaria

(2) ASTRON, Oude Hoogeveensedijk 4, 7991 PD Dwingeloo, The Netherlands

(3) DIAS, Dublin 2, Ireland.

(4) CAS, ESS-USTC, Hefei 230026, China

Abstract

Radio emission of the quiet Sun is considered to be due to thermal bremsstrahlung emission of the hot solar atmosphere. The properties of the quiet Sun in the microwave band have been well studied, and they fit well to the spectrum of bremsstrahlung emission. In the meter-wave and decameter-wave bands, properties of the quiet Sun have rarely been studied due to the instrumental limitations. In this work, we use the *LOw Frequency ARray* (LOFAR) telescope to perform high quality interferometric imaging spectroscopy observations of quiet Sun coronal emission at frequencies below 90 MHz. We present the brightness temperature spectrum, and size of the sun in the frequency range of 20-80 MHz. For the first time, we report about the dark regions with low brightness temperature. The brightness temperature spectrum of the quiet Sun is discussed and compared with the bremsstrahlung emission of the corona model and previous quiet sun observations.

1 Introduction

Radio emission of the quiet Sun has been widely studied in the last few decades. Most prior studies of brightness temperature spectra with spatially resolved observations of the quiet Sun have been carried out in the microwave and centimeter-wave band [1, 2, 3, 4]. More recent works have worked on low frequency quiet sun properties of the sun. Mercier et al. [4] imaged the quiet Sun between 150 and 450 MHz with Nançay Radioheliograph. They obtained the brightness temperatures and the profile in E-W and North-South [N-S] directions. Vocks et al. [5] inferred the scale height temperature of 2.2×10^6 K with LOFAR multi-frequency interferometry imaging. Melnik et al. [6] performed interferometric imaging on the quiet Sun with the Ukrainian T-shaped Radio telescope (UTR-2). [7] achieved the spatial resolution of 0.6 arcmin with lunar de-occultation method with LOFAR HBA in the frequency range of 120-180 MHz, and the measured brightness temperature to be approximately 10^6 K. Detailed and comprehensive studies in lower frequencies (meter-wave and decameter-wave) band have so far not been done, ma-

orly due to instrumental limitations.

The quiet Sun radio emission is interpreted as bremsstrahlung emission in previous studies [2, 8]. Selhorst et al. [8] numerically derived the brightness temperature spectrum in the microwave band with modeled electron and ion density and temperature altitude profile [9, 10]. The result fits the brightness temperature measurements well in the frequency range of 1.5-300 GHz. In lower frequency band, the size of the Sun increases with the wavelength of observation, and the observed brightness temperature is lower than that modeled [4], this is due to the propagation effect, i.e. the refraction and scattering. [11] studied the brightness temperature and size of the Sun with ray tracing simulation, the result indicating that the quiet sun observation results could be significantly influenced by propagation effects. Thus, detailed and comprehensive observation studies on the quiet sun in low frequency band can present the propagation effect of radio waves, and help diagnose the scattering properties and background plasma of solar atmosphere.

In this work, we present the spatial resolved temperature spectrum observed by LOFAR and compare to previous studies and the modeled brightness temperature of quiet sun.

2 Observation and data reduction

We used the LOFAR-LBA [13] outer antennas in Core+Remote observation mode for the quiet Sun observation. In the interferometric observation, 24 core stations and 9 remote stations were included, forming 528 station baselines, from which the longest baseline is 48 km. With simultaneous observation of the Sun and the Cas-A calibrator source, we perform the calibration for the visibility of each baseline using the Default Pre-Processing Pipeline (DPPP) [14]. Considering the static nature of the quiet Sun, we use AOFlagger [15] to flag out the transient varying data frames and radio frequency interference (RFI); this flagging step can significantly improve the quality of imaging for static radio sources. The calibrated visibility in form of

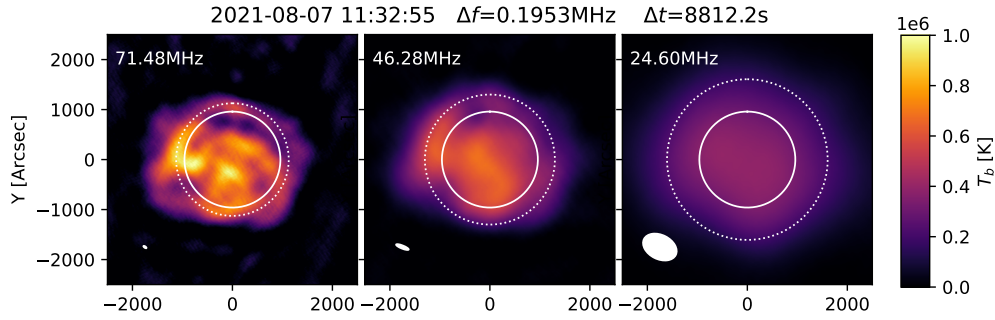


Figure 1. The interferometry imaging of the quiet Sun on 2021-08-07. The beam shape is marked as a white patch in the lower left corner of each panel; solid white lines represents the edge of the optical solar disk; dotted white line represents the local frequency plasma height ($f = f_{pe}(h)$) according to [12] electron density model.

measurement-sets is input into WSClean[16] for the procedures of uv-space sampling, Fourier transformation, and deconvolution. In order to reveal the weak and faint structure in the imaging, we applied the full 2.45 hours' time-integration duration and 0.195MHz frequency averaging to increase signal to noise ratio.

3 Results

From the observations, we obtained one image in each of 45 subbands, Figure (1) presents the brightness temperature distribution of 3 representative subbands. With all the brightness temperature measurements, we can derive (1) the average brightness temperature spectrum of center disk region $r < 0.5R_{Sun}$. (2) the brightness temperature spectrum of a given position (3) the brightness temperature profile on the center line of south to north [S-N] direction and east to west [E-W] direction.

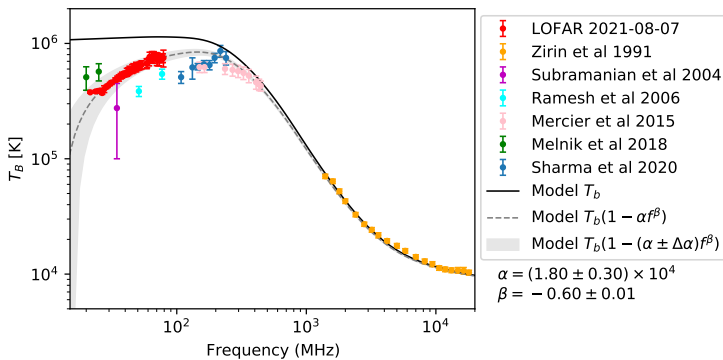


Figure 2. The brightness temperature spectrum of LOFAR on 2021-08-07 (red), and previous works: [2, 3, 17, 4, 6, 18]. The brightness temperature in this work is obtained by averaging the brightness of $r < 0.5R_{Sun}$ region in the imaging of each frequency. The black continuous line is the modeled brightness temperature of bremsstrahlung emission [8]; the gray dashed line is the mean fitted flux attenuation ratio due to propagation effects; the gray shaded area shows the effect of the variation in the fit parameters.

The average brightness temperature (T_b) spectrum (as

shown in Figure 2) obtained in this work is in well consistent with previous works, and the values of T_b is below the model predicted value, the model by Selhorst et al [8] solves the radiation transfer equation in the line-of-sight, considering the bremsstrahlung radiation in the solar atmosphere. While the model didn't consider the radio wave propagation effect (scattering and refraction from the solar atmosphere and interplanetary plasma).

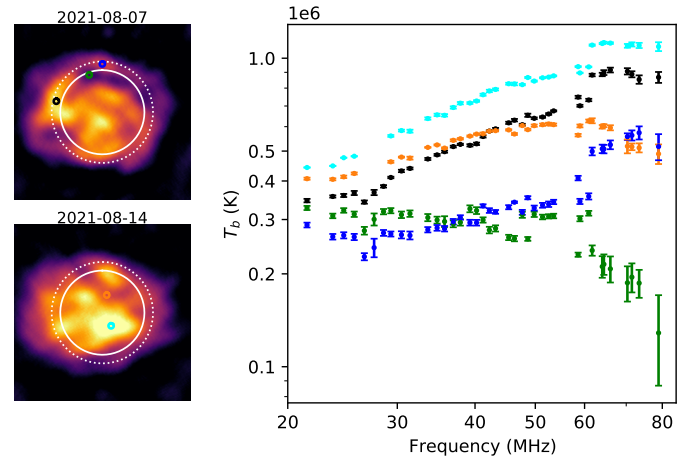


Figure 3. Brightness temperature spectrum of given points on 2021-08-07 and 2021-08-14. Colored circles on the left two panels marks the position of the coordinate points, the size of the circle represents the regime of averaging. The brightness temperature spectrum is shown in the right panel with corresponding color.

With imaging of multi-frequency subbands, we obtained the brightness temperature spectrum of given coordinate points. The five positions in Fig. 3 include five repetitive features: the green point represents the low brightness temperature dark region, the blue represents the bright patch above the Northern-polar coronal hole, black represents the active region on the limb, the orange represents the active region near the disk, the cyan represents the bright equatorial coronal hole. We observed brightness temperature as low as 0.13 MK on the solar disk near 80MHz. The spectrum varies largely for different locations on the solar disk.

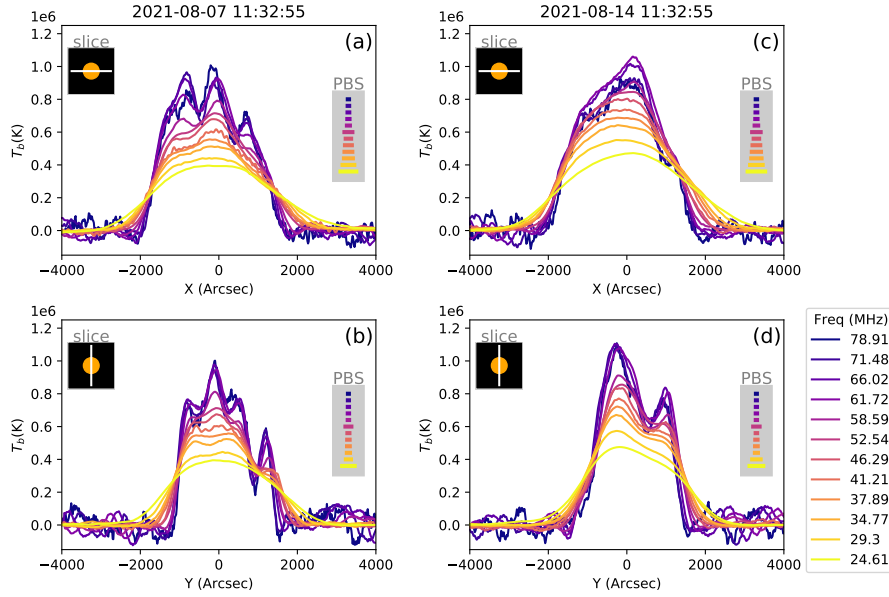


Figure 4. Slices of brightness temperature distribution along the center line of longitude and latitude. Projected beam size (PBS) represents the beam-size projected to the slice line.

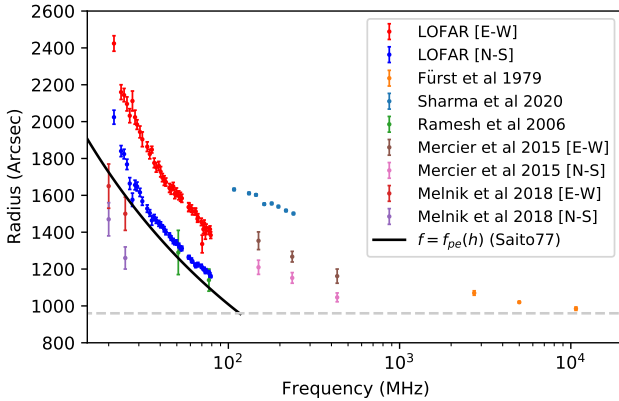


Figure 5. The radius of the Sun measured as the half-width half-maxima across the observed frequency band on 2021-08-07. The black line represents the local plasma radius from the density model of [12], and the gray dashed line represents the optical radius. Results from other studies are given for comparison.

We obtained the radius of quiet Sun in 45 subbands. As shown in Figure 5. The width in the horizontal [E-W] direction is significantly larger than the width in the vertical [N-S] direction. This can be related to the larger plasma density of the active regions and coronal streamers in the low-middle latitude with respect of the plasma density of the coronal holes in the polar region. The radius observed by LOFAR follows the same trend as the local plasma radius ($f = f_{pe}(h)$). The N-S radius is very close to local plasma radius. Comparing with previous observations, the N-S radius is well consistent with MWA observations of quiet Sun equator by [17]. Both E-W and N-S radii are significantly

larger than the result of [6]. The trend of radius-frequency to high frequency is consistent with [4] and smaller than that by [18].

4 Summary

In this work, we use LOFAR-LBA to observe the quiet Sun. The major results include:

- We measured the disk center brightness temperature and the radius of the quiet Sun in frequency range of 20-80MHz.
- The brightness temperature is consistent with previous work in this frequency range but lower than modeled values. We assume the difference is due to propagation effects. The brightness temperature on 2021-08-07 could be fitted by $T'_b(f) = T_b(f)(1 - \alpha f^\beta)$ with $\alpha = (1.80 \pm 0.30) \times 10^4$ and $\beta = -0.60 \pm 0.01$.
- The radius of the quiet Sun is measured as half power of maximum. The results are consistent with previous measurements: the radius in E-W direction is larger than that in N-S direction, and both are larger than the local plasma frequency radius.

The brightness temperature and size observations in this work provides a reference for future parametric simulation works. More comprehensive observation-targeted parametric simulation works could help diagnosing the plasma background by searching for the best match parameter combinations to reproduce the observations.

References

- [1] E. Fürst, W. Hirth, and P. Lantos, “The radius of the sun at centimeter waves and the brightness distribution across the disk,” *Solar Physics*, vol. 63, no. 2, pp. 257–270, 1979.
- [2] H. Zirin, B. Baumert, and G. Hurford, “The microwave brightness temperature spectrum of the quiet sun,” *The Astrophysical Journal*, vol. 370, pp. 779–783, 1991.
- [3] K. Subramanian, “Brightness temperature and size of the quiet sun at 34.5 mhz,” *Astronomy & Astrophysics*, vol. 426, no. 1, pp. 329–331, 2004.
- [4] C. Mercier and G. Chambe, “Electron density and temperature in the solar corona from multifrequency radio imaging,” *Astronomy & Astrophysics*, vol. 583, p. A101, 2015.
- [5] C. Vocks, G. Mann, F. Breitling, M. Bisi, B. Dąbrowski, R. Fallows, P. Gallagher, A. Krankowski, J. Magdalenic, C. Marqué *et al.*, “Lofar observations of the quiet solar corona,” *Astronomy & Astrophysics*, vol. 614, p. A54, 2018.
- [6] V. Melnik, V. Shepelev, S. Poedts, V. Dorovskyy, A. Brazhenko, and H. Rucker, “Interferometric observations of the quiet sun at 20 and 25 mhz in may 2014,” *Solar Physics*, vol. 293, no. 6, pp. 1–10, 2018.
- [7] A. M. Ryan, P. T. Gallagher, E. P. Carley, M. A. Brentjens, P. C. Murphy, C. Vocks, D. E. Morosan, H. Reid, J. Magdalenic, F. Breitling *et al.*, “Lofar imaging of the solar corona during the 2015 march 20 solar eclipse,” *Astronomy & Astrophysics*, vol. 648, p. A43, 2021.
- [8] C. Selhorst, A. Silva, and J. Costa, “Solar atmospheric model with spicules applied to radio observation,” *Astronomy & Astrophysics*, vol. 433, no. 1, pp. 365–374, 2005.
- [9] J. Fontenla, E. Avrett, and R. Loeser, “Energy balance in the solar transition region. iii-helium emission in hydrostatic, constant-abundance models with diffusion,” *The Astrophysical Journal*, vol. 406, pp. 319–345, 1993.
- [10] A. Gabriel, “The solar corona,” in *The Sun: A Laboratory for Astrophysics*. Springer, 1992, pp. 277–296.
- [11] G. Thejappa and R. MacDowall, “Effects of scattering on radio emission from the quiet sun at low frequencies,” *The Astrophysical Journal*, vol. 676, no. 2, p. 1338, 2008.
- [12] K. Saito, A. I. Poland, and R. H. Munro, “A study of the background corona near solar minimum,” *Solar Physics*, vol. 55, no. 1, pp. 121–134, 1977.
- [13] M. á. van Haarlem, M. Wise, A. Gunst, G. Heald, J. McKean, J. Hessels, A. De Bruyn, R. Nijboer, J. Swinbank, R. Fallows *et al.*, “Lofar: The low-frequency array,” *Astronomy & astrophysics*, vol. 556, p. A2, 2013.
- [14] G. van Diepen, T. J. Dijkema, and A. Offringa, “Dppp: Default pre-processing pipeline,” *Astrophysics Source Code Library*, pp. ascl–1804, 2018.
- [15] A. Offringa, J. Van De Gronde, and J. Roerdink, “A morphological algorithm for improving radio-frequency interference detection,” *Astronomy & astrophysics*, vol. 539, p. A95, 2012.
- [16] A. Offringa, B. McKinley, N. Hurley-Walker, F. Briggs, R. Wayth, D. Kaplan, M. Bell, L. Feng, A. Neben, J. Hughes *et al.*, “Wsclean: an implementation of a fast, generic wide-field imager for radio astronomy,” *Monthly Notices of the Royal Astronomical Society*, vol. 444, no. 1, pp. 606–619, 2014.
- [17] R. Ramesh, H. Nataraj, C. Kathiravan, and C. V. Sastri, “The equatorial background solar corona during solar minimum,” *The Astrophysical Journal*, vol. 648, no. 1, p. 707, 2006.
- [18] R. Sharma and D. Oberoi, “Propagation effects in quiet sun observations at meter wavelengths,” *The Astrophysical Journal*, vol. 903, no. 2, p. 126, 2020.